On the Generation of Ocean Wind Waves as Inferred from Airborne Radar Measurements of Fetch-Limited Spectra[1]

T. P. Barnett[2] and J. C. Wilkerson

U. S. Naval Oceanographic Office

ABSTRACT

A section of sea surface that had been subjected to a constant offshore wind was profiled by using an airborne radar-wave profiler. The profiles extended seaward from the coast for a distance of 350 km. From these data, estimates of the spectrum of encounter of the sea surface were obtained for different fetch lengths. It was possible to retrieve the true wave spectrum as a function of fetch length. Spectral growth curves were then obtained and analyzed in light of recent theories on wave generation. The data are consistent with the resonance theory of wave growth (Phillips 1957), provided the magnitude of the mean-square atmospheric pressure fluctuations are 50 times greater than those given by Priestley (1965) for low wind speeds over land. The data also suggest that wave growth through an instability mechanism (e.g., Miles 1957) is yet to be understood. Both of these conclusions support similar findings of Snyder and Cox (1966). It was found that higher-frequency waves grow past or "overshoot" their eventual equilibrium energy value. After overshooting, they then rapidly decay back to an equilibrium range.

1. *Introduction.* Why waves form when air flows over water is a question that has not been satisfactorily answered, but several theories that could account for wave generation have been advanced. With the exception of the measurements by Snyder and Cox (1966), it has not been possible thus far to adequately observe the manner in which the wind actually adds energy to the wave spectrum. Hence, the theories are almost untested. Recently, the U.S. Naval Oceanographic Office has initiated a series of field experiments designed to measure the rate of growth of the energy spectrum under steady-wind conditions. This paper describes the method and results of the first of these experiments and compares the data obtained with recent theoretical results.

In this experiment we have observed steady-state fetch-limited wave spectra that had been developed by a geophysically uniform wind field at a number

1. Accepted for publication and submitted to press 18 May 1967.

2. Present address: Westinghouse Ocean Research Laboratory, San Diego, California.

of different fetch lengths. From these observations it was possible to obtain estimates of spectral growth. In practice, the observations were timed to take place after the offshore winds behind a strong low-pressure system had established a stationary wave system within approximately 275 km of the eastern coast of the United States. An aircraft, equipped with a high-resolution radar altimeter, then obtained continuous profiles of the sea surface from the coast seaward to a desired distance, first in a downwind direction and then upwind. The data were subsequently transformed into spectra that were representative for various distances from the coast. These spectra eventually provided the basis for estimates of spectral growth over the major frequency range of the spectrum. A critical factor in the analysis was the constancy of the wind field during, and for a given time before, the flight.

2. *General Theory and Background.* The method employed in reducing the sea surface profiles to the final estimates of real spectral growth is discussed in § 6. Here we consider pertinent background information and general theoretical approach.

Several workers have independently proposed the following general equation to describe the energy balance of the wave spectrum in deep water:

$$\frac{\partial F}{\partial t}(\sigma, \varphi, \vec{x}, t) + \vec{V}_g \cdot \vec{\nabla} F(\sigma, \varphi, \vec{x}, t) = G; \tag{1}$$

here $F(\sigma, \varphi, \vec{x}, t)$ is the local energy spectrum at position $\vec{x}$ and time t; $\vec{V}_g$ (σ, φ) is the group velocity of the component with circular frequency σ $[= (gk)^{1/2}]$ and relative direction φ; and the function G represents all processes that add energy to, or subtract energy from, F. The complete G-function is not presently known, but it is possible to define a linear form of G that will be adequate for our immediate purposes (Hasselmann 1960):

$$G \approx \alpha + \beta F; \tag{2}$$

α and β correspond to wave growth mechanisms that are linear and exponential in time (space); respectively, such mechanisms might be explained by the resonance theory of Phillips (1957) and the shear-flow theory of Miles (1957). Reviews of these theories have been given (e.g., by Longuet-Higgins et al. 1963). If G is given by (2), then (1) is a linear form of the energy equation and will be considered valid until nonlinear and/or dissipative effects take over.

It is clear that an appropriate form of (1) can be used to obtain estimates of α and β, provided one of the three following conditions can be fulfilled during the initial growth phase:

(i) if $F(\sigma, \varphi, \vec{x}, t)$ and $\vec{W}(\vec{x}, t)$ are known for sufficient t and $\vec{x}$;

(ii) if $F(\sigma_0, \varphi_0, t)$ and $\vec{W}(\vec{V}_g t, t)$ are known for sufficient t and $\vec{V}_g$ equals the group velocity of the (σ_0, φ_0) component,

(iii) if $F(\sigma, \varphi, \vec{x})$ and $W(\vec{x})$ are known for sufficient $\vec{x}$ and are stationary for specified t.

The first condition, which essentially estimates α and β by a hindcasting technique, generally involves the solution of a nonlinear integro-differential form of (1). Details of such an analysis have been given by Barnett (1966).

The second condition is identical to the case considered by Snyder (1965) and Snyder and Cox (1966). In their experiment a directional wave recorder was towed at constant speed downwind from Eleuthera Island, Bahamas. A singularity in the spectral transformation, relating the true frequency and direction of a wave component to its apparent frequency and direction, allowed them to estimate the spectral intensity of that component having a group velocity equal to the towing velocity. They obtained spectral growth curves for a single component (wavelength 17 m) over a range of wind speeds. From these data they quantitatively evaluated the relative importance and correctness of the wave-growth theories previously mentioned. Their results supported the resonance theory of Phillips. They also showed that the instability theory of Miles predicts rates of wave growth that are almost an order of magnitude too low.

The final condition is the one met in this work. Expanding on (iii), it is sufficient that the wind field be at least weakly stationary over a reasonably large region encompassing the observation area. The amount of time, t, during which the wind should be stationary depends on the frequency component to be observed and on the fetch distance at which the observation is to be made. This quantity may be approximated by

$$t = \frac{d}{V_g(\sigma)}, \tag{3}$$

with d equal to the maximum fetch distance for which the σ-component would be fully developed and with both d and t sufficiently large (Phillips 1958a). For all frequencies in which (3) is satisfied or in which time for full development is less than that given by (3), with d and σ given, eq. (1) reduces to:

$$\vec{V}_g \cdot \vec{\nabla} F = G. \tag{4}$$

By considering only the steady-state fetch-limited case, we have reduced the data necessary to evaluate α and β to $F(\vec{x})$ and $W(\vec{x})$. Without a large number of ships, oceanographic buoys, or both, collection of even these data would be a nearly impossible task. However, with the relatively fast (100 m/sec) airplane-altimeter arrangement, a means of estimating $F(\vec{x})$ has been provided,

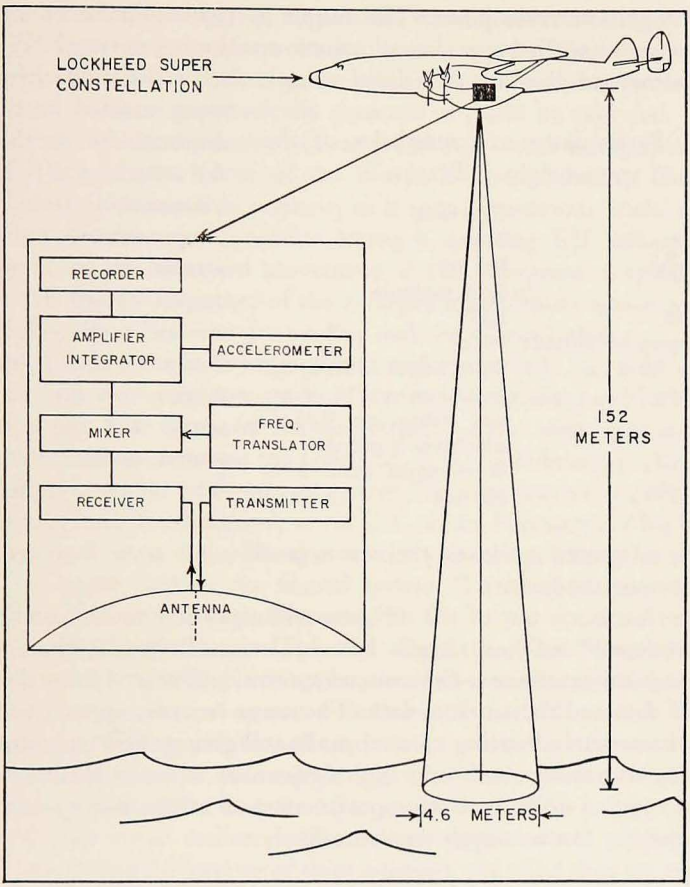

Figure 1. A schematic view of the airborne sea-surface profiler.

and with uniform wind fields, $\vec{W}(\vec{x})$ has been reduced to $\vec{W}$. Both of these simplifications involve certain assumptions that will be justified in later sections.

3. *Instruments.* The airborne radar wave profiler employed is a system under development for the U.S. Naval Oceanographic Office. It is composed of three functional sections: the antenna assembly, the height sensor, and the vertical aircraft-motion sensor. The entire instrument package is mounted near the center of gravity of the aircraft (a Lockheed Super Constellation). Fig. 1 shows a simplified block diagram of the instrument, and Table I lists its more important characteristics. Here the wave profiler is only briefly discussed; for greater details see Barnett and Wilkerson (1967).

Vertical motion of the aircraft is sensed by an accelerometer (range ± 1 g, sensitivity 0.0001 g), which provides a signal to electronic circuitry, where

double integration takes place. The output is representative of aircraft displacement and is applied as a second input to a summing network. With proper scaling factor and phasing, this signal cancels the incremental altitude signal input created by the vertical displacement of the aircraft. All other signals (wave-height information) from the summing network are then forwarded to an amplifier, the output of which is recorded on an oscillograph. Fig. 2 shows an analog trace of the outputs of the wave-height sensor and the doubly integrated accelerometer signal. The rolling and pitching motions of the plane can also introduce unwanted noise to the wave profile, but such motions are relatively unimportant here.

Table I. Performance characteristics of the Amecon wave-height indicator.

Frequency	4300 mc/s
Modulation – FM	25 kc/s
Power output	300 mw
Antenna	Split parabola
Beam width	1.72°
Nominal operating altitude	152 m
Accuracy	Wave height between 0.6 and 15 m, ±10% of actual value, or 0.15 m, whichever is greater
Resolution	Wavelengths from 9 to 600 m

In a performance test of the airborne wave profiler under conditions of a "fully developed" sea near Argus Island Tower, Bermuda, there was good agreement between the one-dimensional spectra determined from the Tower's wave staff data and the airplane data. The wave recorder appeared to be quite capable of accurately locating spectral peaks and giving their magnitude. However, agreement diminished with high frequency; it is not clear whether this was due to system noise or to attempts to compare a time history with a spatial history, but the former seems the more likely.

4. *The Weather.*[3] To attempt significant estimates of a wave spectrum's evolution, the measurements had to be made under ideal wind conditions. An offshore wind of constant velocity should have been blowing over a large area

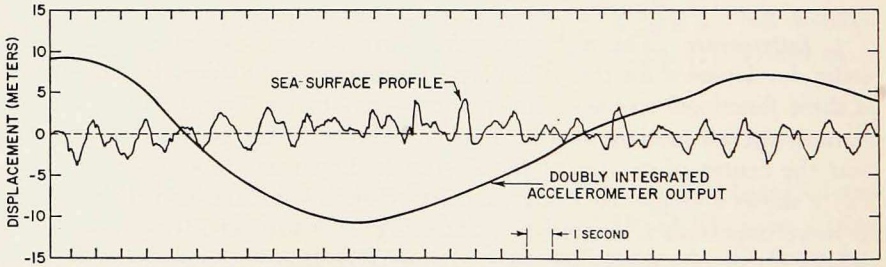

Figure 2. A typical length of profiler record.

3. We are grateful to Lionel I. Moskowitz for providing the general weather analysis.

of the ocean for a given time (§ 2) prior to wave observation. Also, the wind field should have been uniform in its lateral extent. These were difficult conditions to meet, but fortunately, the wind field over and around the observation area was about as geophysically constant as could be expected.

The general weather situation was as follows: A weak low-pressure system (1007 mb), located just north of the North Dakota-Canadian border early on 17 February, developed in intensity as it moved eastward; at the same time a high-pressure system of moderate strength, pushing ESE out of Canada, was accelerating the eastward movement of the low-pressure system. At 00 UT on 18 February the center of the enlarged low-pressure system (1000 mb) was located midway between James Bay and the Great Lakes.

A north-south isobaric configuration, with practically no field curvature, developed to the east of the low-pressure center and remained until after 12 UT on 20 February. The winds off the mid-Atlantic states were light and variable until the frontal system passed the coast (00 UT, 19 February). After passing over New England, the low-pressure system began to intensify rapidly (984 mb in the center over New England, at 00 UT on 20 February). This deepening of the storm led to an intensification of the pressure gradient, increasing the surface-wind speeds behind the frontal system. These winds prevailed in the coastal areas of Maine to Cape Hatteras, N. C.

4.1 The Wind Field in Greater Detail. The National Weather Records Center at Ashville, N. C., has provided the wind details presented in Fig. 3. An A at the base of an arrow indicates that the data were taken with an anemometer. Where possible, all anemometer data have been converted to values at a height of 10 m, assuming a logarithmic profile and considering the drag-coefficient data of De Leonibus (in preparation). This height corresponds to the level that visual estimates taken from shipboard are purported to represent. Considering the variety of ships engaged, the wind data are remarkably uniform. A wind speed of 30 to 35 kts (15.2–17.8 m/sec) and a direction of 335°T are typical of the values reported. The plane track (dashed lines in Fig. 3) was oriented so that it was parallel to the wind direction.

Fig. 4 shows a time history of the wind force and direction at selected nearshore stations where anemometers were used. Since the air mass associated with this storm was very unstable,[4] some variability due to gustiness is present in Fig. 4. But even with this variability the constancy of the nearshore wind field through the measurement time was reasonably good.

For the region far from shore, it was not possible to obtain similar anemometer wind data, but estimates of the wind for this area were obtained through accurate plane positioning. By locating the plane every five minutes with Loran A, the plane's ground speed could be estimated. Since the indicated air speed was maintained constant during flight, one simple subtraction yielded the effective wind speed. Because of the directions of the wind and plane flight,

4. Air-sea temperature differences as reported by the lightships were between $-6°$ and $-10°$C.

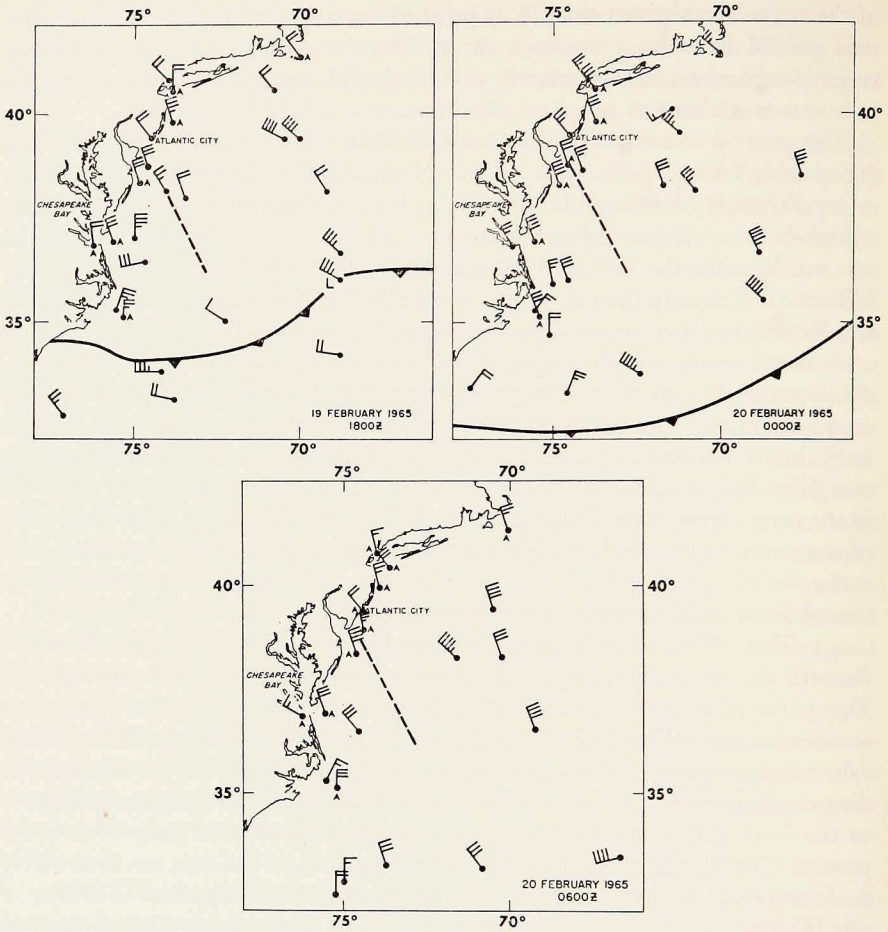

Figure 3. a, b, and c. Sequential wind and weather maps for coastal and offshore areas of the Middle Atlantic states, 18 UT 2-19-25 to 06 UT 2-20-65.

this effective wind speed was practically identical to the true wind speed at the altitude of the aircraft — 152 m above the mean sea surface. The average wind on the downwind run was 33 kts (16.8 m/sec), on the upwind run, 30 kts (15.2 m/sec). These values are a bit lower than the actual wind speed, since the plane did not fly a precisely straight line out from the coast.

To obtain an estimate of the uniformity of the wind field with distance from the coast, values of the wind speed were calculated by using successive five-minute LORAN positions. The smoothed results are shown in Table II. The downwind wind speeds show a fairly large variability, because the plane's ground speed of approximately 220 kts (112 m/sec) gave rise to a

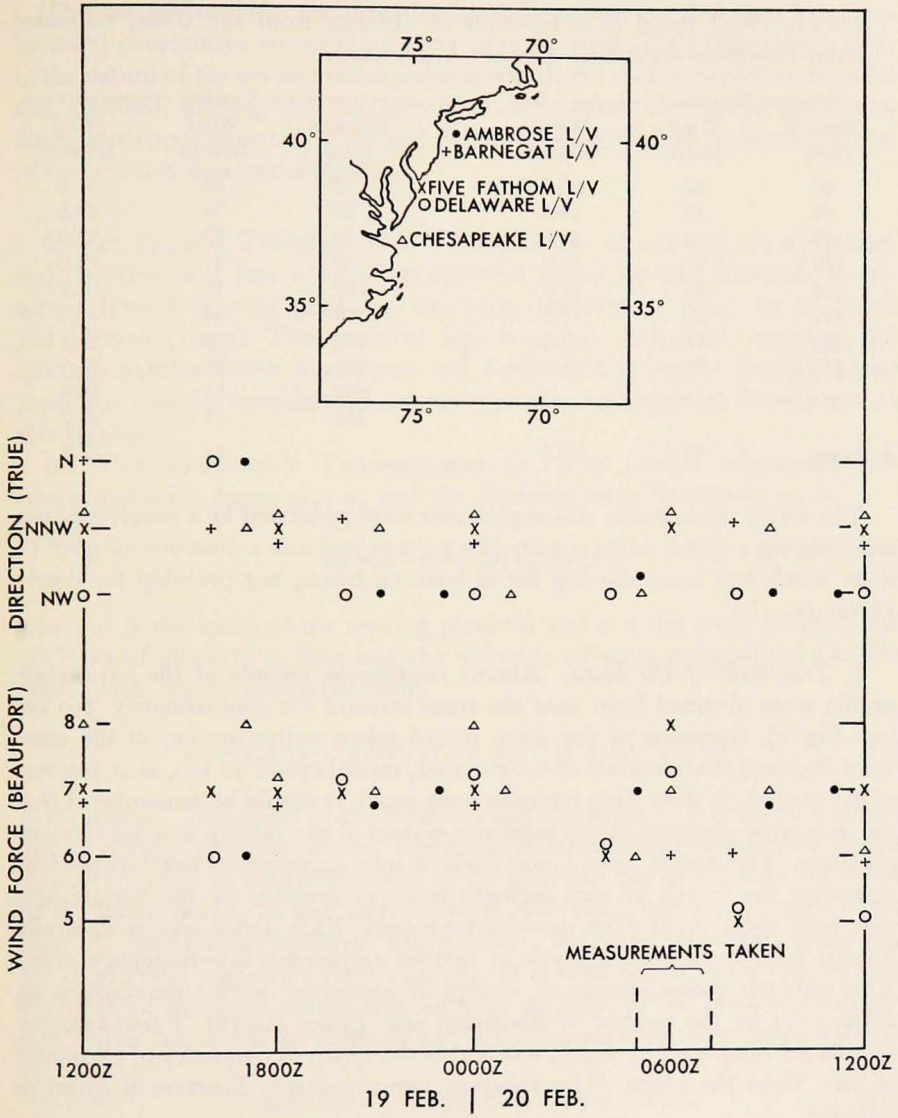

Figure 4. Time histories of wind force and direction at ocean light ships off the Middle Atlantic states.

larger positioning error. The upwind wind speeds were more uniform, since the approximate ground speed of the plane here was 150 kts (76 m/sec). The data show that the wind field was uniform with respect to distance from the coast. No attempt has been made to reduce the plane winds to equivalent winds at a height of 10 m.

Table II. Wind speed as a function of distance from the coast, estimated from smoothed sequential LORAN A positions.

Downwind			Upwind		
Distance (km)	Wind (knots)	Wind (m/sec)	Distance (km)	Wind (knots)	Wind (m/sec)
46	40	20.6	33	34	17.5
95	37	19.0	60	34	17.5
143	42	21.6	95	35	18.0
179	37	19.0	128	34	17.5
210	33	17.0	179	30	15.4
247	33	17.0	210	34	17.5
283	44	22.6	247	30	15.4
329	38	19.5	265	36	18.5
			302	33	17.0
			338	47	24.2
Average	38.0	19.5		34.7	17.9

The waves measured in this experiment were generated by a nearly offshore wind having a speed[5] of 34 ± 4 kts (17.3 ± 2 m/sec) and a direction of 335°T; these winds had been blowing for at least 12 hours, but probably for nearly 16 hours.

5. *Treatment of the Data.* Almost continuous records of the sea-surface profile were obtained from near the coast seaward for approximately 350 km (see Fig. 2). Segments of the wave record taken within 90 km of the coast were digitized at an interval of 0.05 second, those beyond 90 km, at an interval of 0.1 second. If these time intervals seem small, it should be remembered that the data were obtained in the reference system of the rapidly moving airborne platform. The entire record was divided into consecutive but independent segments, the length of each segment being determined by the requirement that each must be at least quasihomogeneous. Each series was numerically filtered prior to spectral analysis to remove extraneous low-frequency noise. The apparent power spectra or spectra of encounter were computed on an IBM 7074 by the method of Blackman and Tukey (1958). These apparent spectra are designated by $E(\omega)$, where ω is the apparent frequency of encounter as seen from the plane. The apparent autocorrelation function is given as follows:

$$r(\tau) = \langle h(t)\, h(t+\tau) \rangle,$$

with $h(t)$ being the time history of the sea surface as seen from the aircraft. The spectrum of encounter is:

$$E(\omega) = 1/\pi \int_0^\infty r(\tau) \cos \omega\tau \, d\tau.$$

5. Referred to the altitude of the aircraft, 152 m.

The raw spectra were corrected for instrument response and then smoothed by using consecutive weighting factors of 0.23, 0.54, 0.23 (hamming). Due to the nature of the sea and the manner in which the measurements were made and digitized, aliasing did not introduce difficulties. The 90% confidence limits were approximately 0.70 and 1.30, differing slightly between the sets of upwind and downwind spectra.

6. *The Spectral Transformation.* The problem of relating the frequency and direction of a free wave to its apparent frequency and direction, as observed from a moving platform, has been discussed in detail by St. Denis and Pierson (1953). The practical aspects of the frequency mapping and spectral transformation have been put forth by Cartwright (1963), whose paper has been of considerable assistance in the mathematical formulation in this section.

6.1 The Frequency Transformation. The unique relationship between real-wave frequency, σ, and the apparent-wave frequency, ω, is

$$\omega = \sigma - (\sigma^2 V/g) \cos \psi, \tag{5}$$

where V is the speed of the moving platform and ψ is the angle between the direction of platform motion and the direction of wave propagation. On the other hand, the inverse relationship

$$\sigma = \{1 \pm [1 - (4\omega V/g) \cos \psi]^{1/2}\}/[(2V/g) \cos \psi] \tag{6}$$

is nonunique. The speed of the platform and the value of ψ determine which branch of (6) is to be considered. The problem is somewhat complicated for the general situation in which the speed of the platform can be less than the speed of the fastest wave. In our case, however, the plane was going much faster than the fastest wave observed. Furthermore, the plane was seeing what was for all practical purposes a pure wind sea. It is most reasonable to assume that nearly all of the wave energy was confined to $\pm 90°$ of the mean wind direction. From (5), ω will be negative and it is convenient to redefine ω and σ as

$$\omega = -\sigma + (V\sigma^2/g) \cos \psi, \quad |\psi| < \pi/2, \tag{5a}$$

$$\sigma = \frac{\{1 + [(4\omega V/g) \cos \psi]^{1/2}\}}{(2V/g) \cos \psi}, \quad |\psi| < \pi/2. \tag{6a}$$

6.2 Specifications of the Integral Transform. The relationship between the apparent spectrum, $E(\omega)$, and the real two-dimensional spectrum relative to the plane heading, $F(\sigma, \psi)$, may be expressed in either of two forms:

$$E(\omega) = \int_{c_1} F(\sigma, \psi) \left| \frac{\partial \psi}{\partial \omega} \right| d\sigma, \tag{7}$$

or

$$E(\omega) = \int_{c_1} F(\sigma, \psi) \left| \frac{\partial \sigma}{\partial \omega} \right| d\psi, \tag{8}$$

where c_1 indicates that the integration is to be carried out over all σ and ψ that can yield the specified value of ω (Cartwright 1963). In the case of the plane traveling downwind, σ and ψ together must satisfy (5a) and (6a), with ω fixed.

To obtain a solution of (7) and (8) it was necessary to represent the two-dimensional spectrum as a product of a frequency-dependent function and an angular spreading factor,

$$F(\sigma, \psi) = H(\sigma) K(\sigma, \psi).$$

In this experiment the plane tracks were only upwind or downwind; therefore it was not possible to obtain direct estimates of $K(\sigma, \psi)$. Hence, it was necessary to make various assumptions concerning this function and then see how sensitive the results were to these assumptions. Three forms of K were considered:

(i) $$K(\sigma, \psi) = K_1(\psi) = \delta(\psi),$$

(ii) $$K(\sigma, \psi) = K_2(\psi) = \frac{8}{3\pi} \cos^4 \psi, \quad |\psi| < \pi/2,$$
$$= 0 \qquad\qquad , \quad |\psi| \geq \pi/2,$$

(iii) $$K(\sigma, \psi) = K_3(\sigma, \psi) = a(\sigma) \cos^{p(\sigma)} \psi, \quad |\psi| < \pi/2,$$
$$= 0 \qquad\qquad , \quad |\psi| \geq \pi/2.$$

Each of the K's has been centered on the plane's heading, which, since it was essentially downwind, is considered to be relative zero. K_1 is a delta function and is equivalent to an assumption that all of the waves were traveling directly downwind. K_2 gives an angular spread that is independent of frequency and is normalized so that

$$\int_{-\pi/2}^{+\pi/2} K_2(\psi) d\psi \equiv 1.$$

The actual directional properties of the spectrum seem to lie somewhere between these two forms. Hence, we constructed a third spreading factor that

had the essential directional properties found by both Longuet-Higgins et al. (1963) and Cote et al. (1960): Waves moving at nearly the speed of the wind ($W/c \sim 1$) were concentrated in a rather narrow angular beam about the wind direction ($\psi = 0$). The width of this beam increased as the ratio of wind speed to wave speed increased. In the definition of K_3, the exponent $p\,(\sigma)$ will be large for $W/c \sim 1$ and will diminish as W/c increases. In Fig. 5 the function $p\,(\sigma)$ is shown versus W/c and compares well with the results of Longuet-Higgins et al. (1963) as amended by Cartwright (personal communication). The normalizing factor, $a\,(\sigma)$, has been chosen so that

$$\int_{-\pi/2}^{+\pi/2} K_3(\sigma, \psi)\, d\psi \equiv 1;$$

therefore

$$a^{-1}(\sigma) = \int_{-\pi/2}^{+\pi/2} \cos^{p(\sigma)} \psi \, d\psi.$$

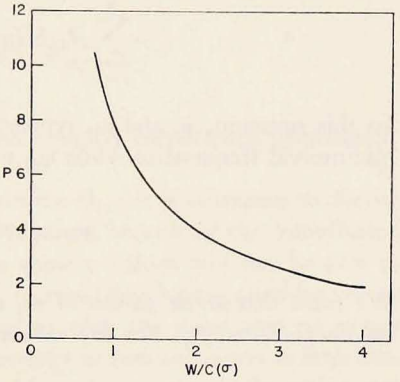

Figure 5. Exponent of spectral directionality, p, versus $W/c\,(\sigma)$ for the K_3 assumption.

To estimate the effect of different directional assumptions, the integral eqs. (7) and (8) were solved for all three of the K's. It should be noted that, in carrying through these solutions, it has been assumed that each K is independent of fetch.

6.3 Solution of the Integral Equations. This section outlines the solution of (7) and (8). Although the present discussion, as before, concerns only the case of a plane traveling downwind, it applies equally well to the upwind case, provided ω, ψ and $K(\sigma, \psi)$ are defined properly.

Substituting for $F(\sigma, \psi)$ and the Jacobians,

$$E(\omega) = \int_{c_1}^{\infty} \frac{H(\sigma)\,[K(\sigma,\psi) + K(\sigma,-\psi)]\, d\sigma}{(\sigma^2 V/g)\,|\sin\psi|}, \tag{7a}$$

and

$$E(\omega) = \int_{c_1}^{\infty} \frac{H(\sigma)\,[K(\sigma,\psi) + K(\sigma,-\psi)]\, d\psi}{[1 + (4\omega V/g)\cos\psi]^{1/2}}. \tag{8a}$$

The problem of solving (7a) or (8a), which are similar to Fredholm integral equations of the first kind, can be considered as a generalization of the problem of solving a set of n-algebraic equations in n-unknowns. Thus (7a) may be approximated as follows:

$$E(\omega_i) = \int_{c_1} \frac{H(\sigma)\,[K(\sigma,\psi) + K(\sigma,-\psi)]\,d\sigma}{(\sigma^2 V/g)\,|\sin\psi|},$$

$$= \sum_{j=1}^{n} \frac{H(\sigma_j)\,[K(\sigma_j,\psi_{ij}) + K(\sigma_j,-\psi_{ij})]\,\delta\sigma_j}{(\sigma^2_j V/g)\,|\sin\psi_{ij}|}, \tag{9}$$

$$= \sum_{j=1}^{n} A_{ij} H(\sigma_j).$$

In this notation, σ_j and ω_i represent individual members of a discrete set of midinterval frequencies while ψ_{ij} is the value of ψ determined by

$$\psi_{ij} = \cos^{-1}\left[\frac{(\sigma_j + \omega_i)g}{\sigma^2_j V}\right].$$

We must determine values of ω_i and σ_j, and, with ψ_{ij} from above, evaluate the coefficients A_{ij}. For the values of σ_j and ω_i for which

$$\psi - \delta\psi < 0 < \psi + \delta\psi,$$

A_{ij} must be evaluated from (8a) due to the singular nature of (7a) at $\psi = 0$. In this case, $H(\sigma)$ varies but slightly over the above interval in ψ; therefore $H(\sigma)$ may be considered as constant in that range (Cartwright 1963). Hence, (8a) is approximated by

$$E(\omega_i) = \frac{H(\sigma^1)}{[1 + (4\omega_i V/g)]^{1/2}} \int_0^{\delta\psi} [K(\sigma^1,\psi) + K(\sigma^1,-\psi)]\,d\psi, \tag{10}$$

where σ^1 is the given value of σ_j determined from the discrete σ-set for which ψ_{ij} at ω_i is nearest to zero. The desired value of A_{ij} may be readily calculated. Values of $\sigma_j < \sigma^1$ cannot give a contribution to E at the particular ω_i, hence the corresponding coefficients of A-matrix must be zero. The final result is a set of n-linear algegraic equations in n-unknowns:

$$[E(\omega_i) - \sum_{j=1}^{n} A_{ij} H(\sigma_j) = 0], \quad i = 1, 2, \ldots, n. \tag{11}$$

The E's are given and the terms of the coefficient matrix, A_{ij}, have been determined in the most appropriate manner.

We must now solve these equations for the desired unknowns, $H(\sigma_j)$. This is not as easy as it may appear, for the set of algebraic equations may be "ill-conditioned", which is another way of saying that various equations may be dependent, or nearly so. A simple test for ill-conditioning has been given

by Redish (1961). Geometrically stated, the test is as follows: Each equation of set (11) may be considered as representing a hyperplane. If two or more of these hyperplanes are nearly parallel, the set is said to be ill-conditioned. To calculate the actual angle between the hyperplanes, the equations were first normalized so that the new coefficients, say A^1_{ij}, are the direction cosines of the normals to the hyperplanes. The angle Θ_{lm} between the l^{th} and m^{th} hyperplanes can be calculated, since

$$\Theta_{lm} = \cos^{-1}\left[\sum_{j=1}^{n} A^1_{lj} A^1_{mj}\right].$$

The nearer the angle Θ_{lm} is to zero, the more poorly conditioned (dependent) are the l^{th} and m^{th} equations.

To suitably condition (11) and thus maximize Θ_{lm}, it is necessary to choose the values σ_j in a judicious manner. This is required because of the complicated relationships between σ and ω and because some σ values will not be able to contribute to the whole range of ω. Hence, to avoid developing quasidependent or redundant equation pairs, it is necessary to pick the σ_j so that no one σ interval will contribute the *majority* of the energy in two successive ω intervals. The equations that finally result form a triangular array of dimension 30, and, because of the finite difference approximation, they represent the original integral equation plus a slight perturbation term. For the integration intervals used in this paper, the perturbation term introduced errors of less than 5% to the solution of (11).

6.4 Definition of the Spectral Field. In presenting the final estimates of spectral energy at various distances from the coast, it has been convenient to speak in terms of true frequency, $f = \sigma/2\pi$, and the true frequency spectrum, $F(f, \psi, x) = 2\pi F(\sigma, \psi, x)$. Figs. 6 and 7 show contours of the quantity $F(f, o, x)$ for the various directional assumptions and the two-plane headings. This is similar to the type of presentation that has been used by Munk and his co-workers in tracking swells from distance storms (e.g., Munk et al. 1963). *Henceforth, all reference to the spectrum will be directed toward the quantity* $F(f, o, x)$.

The contours on each f–x diagram are based on approximately 22 values of F vs f for each of 27 to 30 different x's (600 points/diagram). The x axis is directed downwind, and x equals zero at the coastline. The grid spacing along the x axis was 6.5 km for the region within 90 km of the coast and 13 km beyond. Along the f axis, the grid spacing decreased from 0.011 cps near $f \approx 0.20$ cps. The purpose of this contouring was to show details with a minimum of smoothing, thus presenting the data as objectively as possible. Unfortunately, no data were obtained for the area between about 27 and 46 km from the coast, and this hiatus makes it impossible to discuss the growth of the higher-frequency waves.

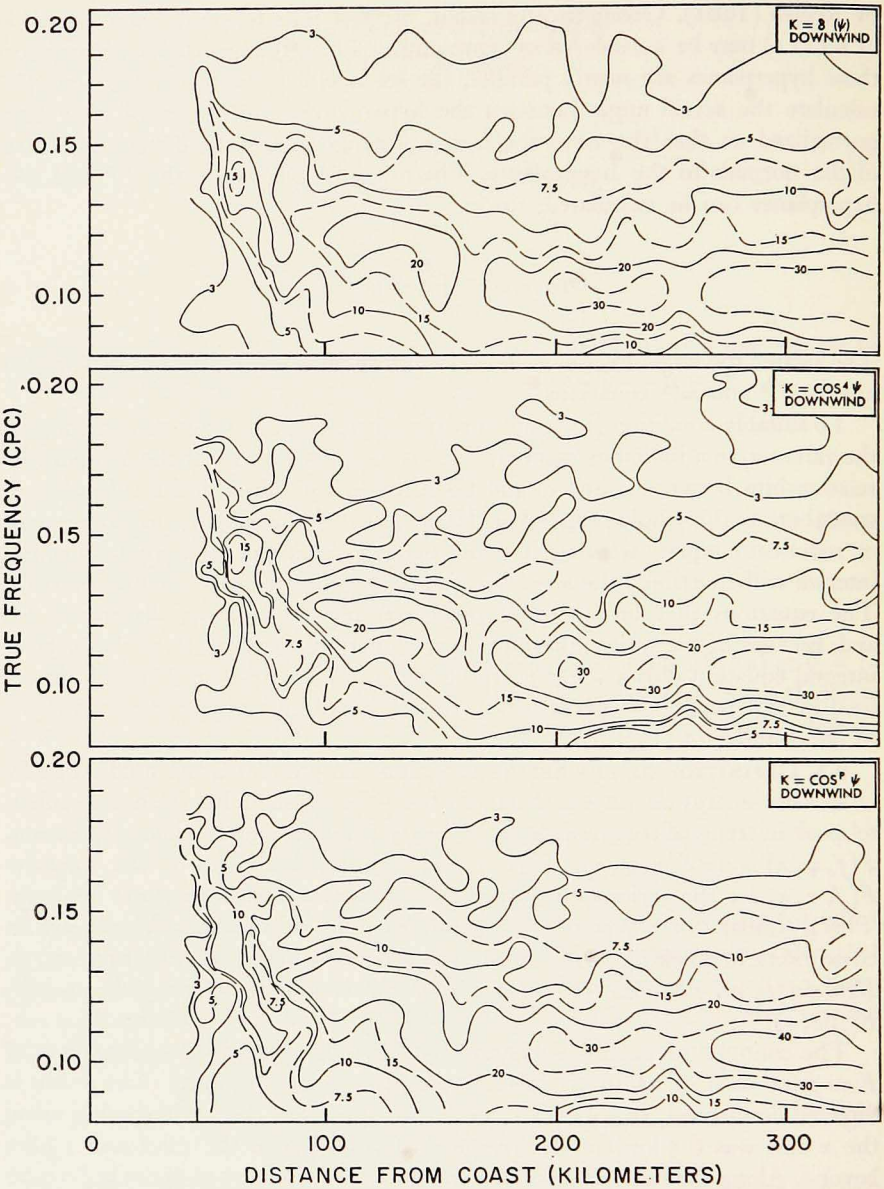

Figure 6. Contours of equal spectral density (m²-sec) on a frequency-distance plot for the downwind run and various directional assumptions.

In viewing the f–x diagrams there are several important items to bear in mind. A cut along the f axis at constant x will give the spectrum $F(f, o)$ at x. Similarly, a cut along the x axis at constant f will give the spacial history of

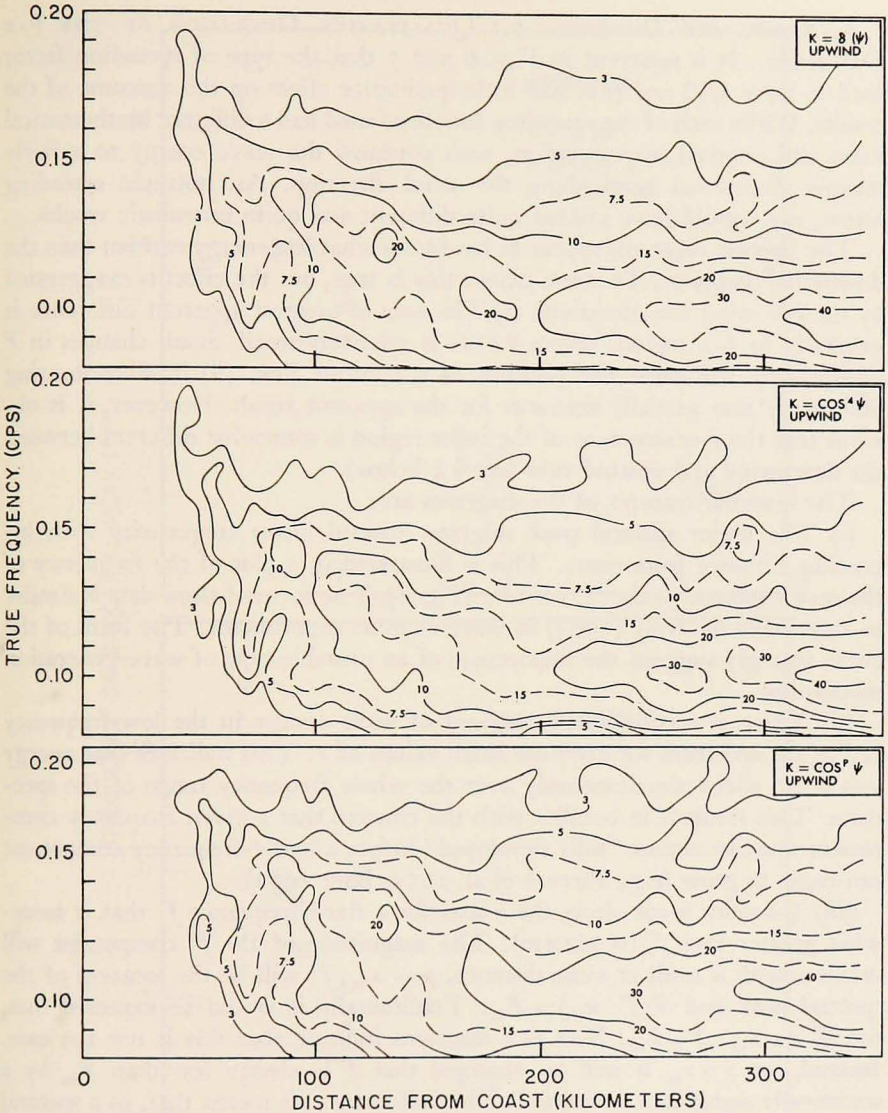

Figure 7. Contours of equal spectral density (m²-sec) on a frequency-distance plot for the upwind run and various directional assumptions.

the f-spectral component. Also of interest is the location of spectral peak(s) or valley(s) at any particular x value and of the value of x beyond which a specified spectral component may be considered to be in equilibrium. In one case, $\partial F / \partial f = 0$ and the tangent to a particular F contour will be parallel to the f axis. In the other case, for an equilibrium condition, $\partial F / \partial x = 0$ and the contour tangent will be parallel to the x axis.

7. *Results and Discussion.* 7.1 Qualitative Discussion of the f–x Diagrams. It is apparent in Figs. 6 and 7 that the type of spreading factor used to solve (7a) and (8a) had little qualitative effect on the outcome of the results. While each of the spreading functions used had a different mathematical form and physical interpretation, each confined the wave energy to a fairly narrow directional band about the wind direction. An isotropic spreading factor, say, would have yielded quite different and quite unrealistic results.

The upwind diagrams appear to have somewhat less energy content than the downwind diagrams. To some extent this is true, but the effect is exaggerated by the following considerations. (i) The area of greatest apparent difference is generally in f–x regions where $\partial F/\partial x$ is relatively small. Small changes in F significantly influence the position of a contour line. (ii) The contouring philosophy also partially accounts for the apparent result. However, it is obvious that the f–x structure of the inner region is somewhat different between the downwind and upwind runs (see § 4 below).

The essential features of the diagrams are:

(i) The major spectral peak migrates toward lower frequencies with increasing distance from shore. This is illustrated in a plot of the frequency of the major spectral peak, f_0, versus x (Fig. 8). The form of these data is similar to that found by Hidy (1965) in wave-channel experiments. The form of the curve strongly suggests the importance of an unstable type of wave-generation mechanism.

(ii) There is a considerable amount of wave energy in the low-frequency end of the spectrum for even the small values of x. This indicates that energy was being added simultaneously over the whole frequency range of the spectrum. This result is in conflict with the concept that a given frequency component must be almost "fully developed" before a lower-frequency component can begin to grow (e.g., Pierson et al. 1955, Baer 1962).

(iii) Consider a cut along the x-axis for a fixed frequency f^1 that is somewhat greater than $f_w(= g/2\pi w)$. The magnitude of the f^1 component will increase with x until at some distance, $x = x_m$, f^1 will be the location of the spectral peak and $F(f^1, x_m) = F_m$. Traditionally it would be expected that, for all $x \geq x_m$, $F \geq F_m$. The f–x diagrams indicate that this is not the case. Instead, for $x > x_m$ it will be observed that F is always less than F_m by a statistically significant amount. In physical terms this means that, as a spectral component grows, it apparently overshoots its eventual equilibrium value. Thereafter, the component gives up energy and soon settles down to the final equilibrium value. For the highest frequencies shown on the diagrams, this effect is obscured by the fact that the area in which the overshoot occurs was not sampled. For a more quantitative discussion of the entire phenomena, see § 7.3.

To explain the overshoot behavior of the individual spectral components is beyond the scope of this paper. We might speculate that the phenomenon

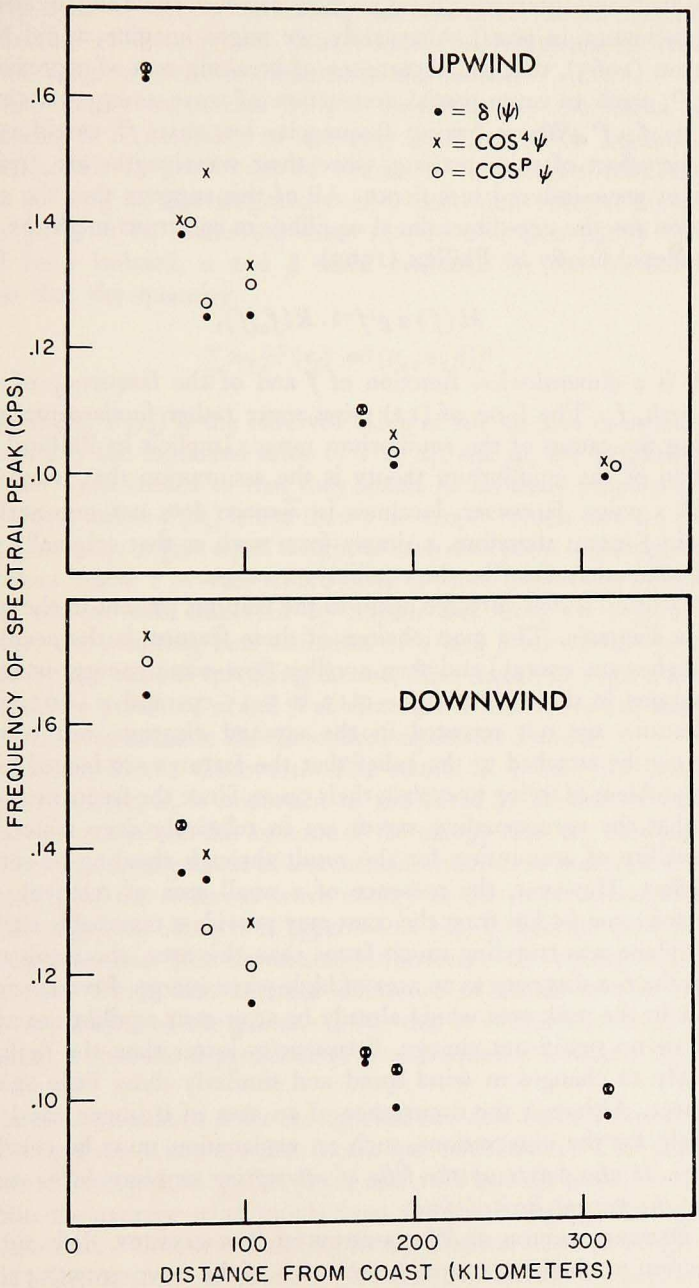

Figure 8. Frequency of the spectral peak as a function of distance from the coast.

is the result of some interaction between the ocean-wave field and the atmospheric field (Hasselmann, in press). Alternately, we might imagine, as did Neumann and Pierson (1963), that the occurrence of breaking seas of approximate frequency, f^1, tends to cause partial destruction of wave energy associated with frequencies $f \geq f^1$. Waves having frequencies less than f^1 would experience little or no effect of this breaking, since their wavelengths are greater than the scale of wave-induced turbulence. All of this suggests that the actual representation for the one-dimensional equilibrium spectrum might be closer to that considered briefly by Phillips (1963):

$$H(f) \propto g^2 f^{-5} \cdot R(f_0/f), \tag{12}$$

where R is a dimensionless function of f and of the frequency of the local spectral peak, f_0. The form of (12) raises some rather fundamental questions concerning the causes of the equilibrium range. Implicit in Phillips' (1958b) formulation of the equilibrium theory is the assumption that wave breaking is local at a point. However, localness in $\vec{x}$-space does not necessarily imply localness in f-space; therefore, a simple form such as that originally proposed need not adequately describe the equilibrium range.

(iv) Attention is now directed again to the features present in the near zone of the f–x diagrams. The most obvious of these features is the occurrence of a peak (high-wave energy) and then a valley (low-wave energy) in the downwind diagrams in the region of $f = 0.12$ to 0.15 cps and $x = 65$ to 80 km. These features are not repeated in the upwind diagram, but considerable certainty can be attached to the belief that the features are indeed real. This raises the problem of trying to explain their cause. Since the frequencies involved indicate that the corresponding waves are in relatively deep water, there is little possibility of accounting for the result through shoaling or some other bottom effect. However, the presence of a small area of relatively stronger wind located some 65 km from the coast may provide a reasonable explanation. Since the plane was traveling much faster than this area, the result would be shown on the f–x diagrams as an area of high-wave energy. Frequencies higher than those in the peak area would already be at or near equilibrium and hence would show no significant change. Frequencies lower than the peak respond more slowly to changes in wind speed and similarly show little evidence of such an area. Although the occurrence of an area of stronger wind accounts qualitatively for the observations, such an explanation must be considered as speculative. *It also points up the folly of attempting anything but a macroscopic analysis of the present limited data.*

7.2.1 Determination of Wave-growth Parameters. It is our purpose in this section to obtain quantitative estimates of the wave-growth parameters, α and β, (2), and to compare these estimates with theory. Before doing so it was necessary to retrieve spectral growth data from the f–x diagrams. This

was simply done by taking cuts along the x-axis at various frequencies. A selected amount of these growth data is shown in APPENDIX A. Also shown are the best-fit growth curves obtained in this section.

Since the theory expounded in § 2 concerns only the linear phases of wave growth, it is necessary to use only data for which nonlinear effects have been small. A good rule of thumb is to consider nonlinearities as negligible so long as the magnitude of a particular spectral component is less than 30% of its maximum value (Snyder and Cox 1966). Once these data had been isolated, α and β were evaluated by the method of least squares so that the quantity

$$\sum_i w_i [F(x_i) - S(x_i, \alpha, \beta)]^2$$

was a minimum. $F(x_i)$ is the observed value of the spectral component at the position x_i, S is the estimated value of F at x_i, and w_i are weighting factors. The w_i have been chosen so that they would be inversely proportional to the square of $F(x_i)$ unless $F(x_i)$ is less than 1 m^2-sec, in which case $w_i = 1/F(x_i)$. Such a system tends to give equal weight to each data point while discriminating against values below 1 m^2-sec, where noise is more important. A comparable weighting scheme was employed by Snyder and Cox. In Figs. 9 and 10, respectively, the resulting best estimates of α and β are shown versus wave frequency for the various spreading factors. Also shown in Figs. 9 and 10 are the theoretically predicted α and β as discussed in the following sections. No effort was made to estimate the directional aspects of α and β.

7.2.2 LINEAR WAVE GROWTH. The results in § 7.2.1 indicate that the linear growth factor, α, is important in the initial generation of wind waves and in providing a substantial amount of the energy near the eventual spectral peak. However, the magnitude of α is sufficiently small so that it *cannot* account for a majority of the observed wave energy at the more advanced stages of spectral development. Also, it is apparent in Fig. 9 that the choice of directional assumption had little significant influence on the estimates of α for an individual run. There was a factor difference of almost two in the corresponding magnitudes of the estimates, but this is of small concern. The important thing is that the dependence of α on frequency is clearly the same for all three K's.

The maximum value of α for the upwind and downwind runs occurred for waves of frequency 0.100 cps and 0.092 cps, respectively. The phase speeds of these waves are 30 and 33 kts (15.2 and 16.8 m/sec), respectively. It is of interest that the average wind speeds from the plane were 30 kts upwind and 33 kts downwind. While it is tempting to try to relate these seemingly coupled facts, it is more prudent to exercise restraint. As mentioned previously, the wind speed is not known to anywhere near the necessary accuracy. Besides, while we have of necessity assumed a geophysically constant wind field, the

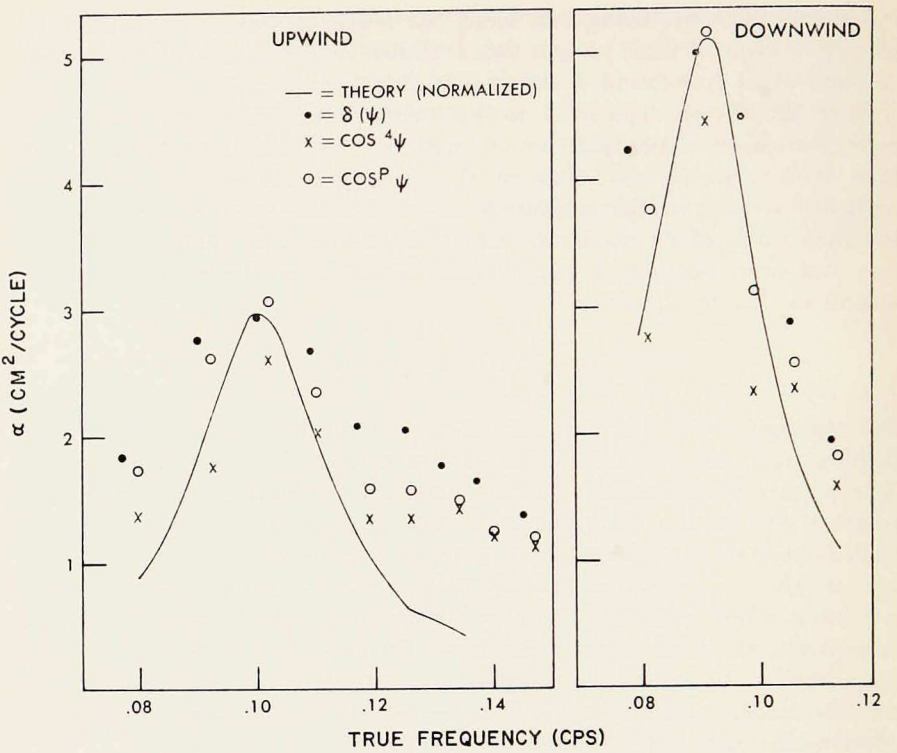

Figure 9. Linear growth parameter, α: Measurement vs the normalized theoretical predictions of Phillips (1957).

actual wind was variable. Therefore the present work can provide only a general averaged picture of the processes of wave generation.

In comparing the observed α's with those predicted by Phillips' theory, it is necessary to estimate the three-dimensional spectrum of atmospheric pressure fluctuations. Priestley (1965) has provided the essential data for such an estimate. His results were first applied by Snyder and Cox (1966) to partially confirm Phillips (1957) theory. The general evaluation of α (suggested by Snyder in a personal communication) in terms of frequency and direction has been given in detail by Barnett (1966); only the results are used here. One problem arises: The expression for the atmospheric pressure spectrum contains a turbulence scaling factor. Priestley's data were obtained for low wind speeds over closely mowed grass, and the corresponding scaling factor was found by Snyder and Cox to be proportional to approximately the fourth power of the wind speed. With such a power law it is possible to extrapolate to higher wind speeds, provided it is assumed that the nature of the turbulent pressure fluctuations was similar during his experiment and ours. However, first esti-

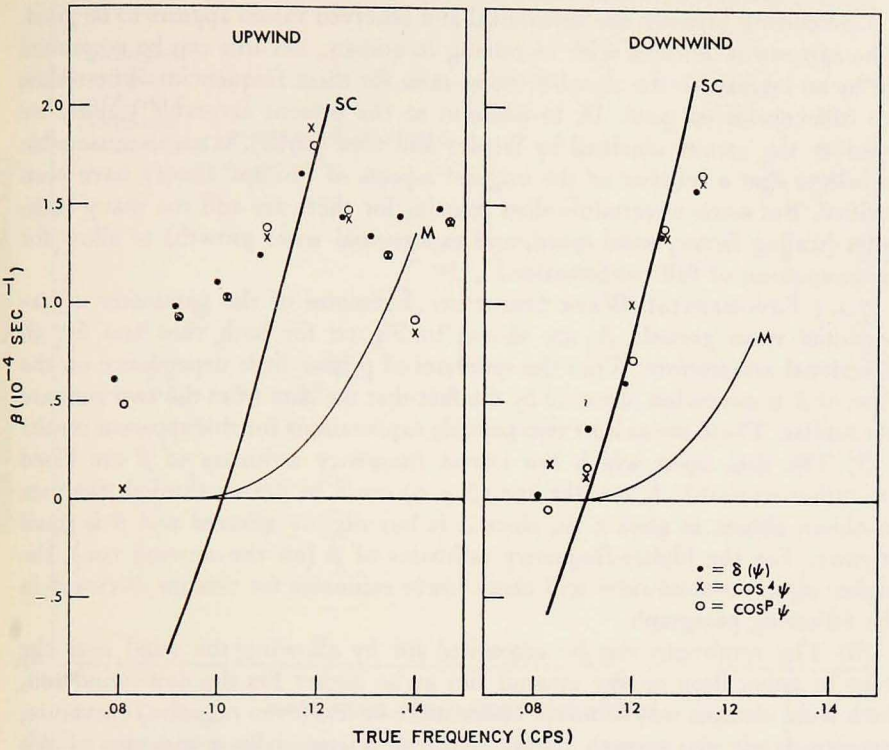

Figure 10. Expotential growth parameter, β: Measurement vs the theory. Curve marked "M" is predicted by Miles (1957) while the line SC is from the empirical relation of Synder and Cox (1966).

mates of α, using such a representation for the scale factor, gave values that were lower than those observed by a factor of approximately 50. It would indeed be fortuitous if the conditions under which Priestley took his limited data could be extrapolated to those of high wind speed accompanied by a rough free-water surface and strong atmospheric instability. To compare the theory of Phillips' with measurement, then, it has been necessary to normalize all theoretical values of α to the magnitude of those observed. Note that, while such normalization changes the magnitude, it does not affect the functional form of α. The *shape* of the curves shown in Fig. 9 are presumably independent of the scaling factor.

The values of wind speed used to evaluate α were 30 kts upwind and 33 kts downwind. These values were selected because they give the best agreement between theory and observation. Since the wind is not known to within the limits implied by these choices, these selections allow the fairest test of the theory.

Comparison between the theoretical and observed values appears to be good. The agreement worsens with increasing frequency, but this can be accounted for by an increase in the signal-to-noise-ratio for these frequencies. The results are still considered good. If, in addition to the present favorable results, we consider the results obtained by Snyder and Cox (1966), it seems reasonable to believe that a number of the original aspects of Phillips' theory have been verified. But some uncertainty does remain, for there are still too many loopholes (scaling factor, wind speed, and exponential wave growth) to allow for an assumption of full confirmation.

7.2.3 Exponential Wave Growth. Estimates of the parameter of exponential wave growth, β, are shown in Fig. 10 for both runs and for all directional assumptions. That the estimates of β have little dependence on the form of K is somewhat obscured by the fact that the data from the two runs are not similar. There are at least two possible explanations for this apparent result:

(i) The data upon which the lowest frequency estimates of β are based are rather scattered. A straight line ($\beta = 0$) could be drawn through the data to obtain almost as good a fit, since α is but slightly affected and β is small anyway. For the higher-frequency estimates of β (on the upwind run), the higher signal-to-noise-ratio will cause lower estimates for reasons discussed in the following paragraph.

(ii) The result can also be accounted for by allowing the wind near the coast to either drop on the upwind run or be higher for the downwind run. Such wind changes would induce either more or less (even negative) curvature, respectively, in the growth curves. Since β is essentially a measure of this curvature, the result could be as shown in Fig. 10. The foregoing discussion serves to re-emphasize the fact that the numerical estimates of β, and to a lesser extent of α, should be considered as order-of-magnitude-values.

Now it is pertinent to compare theory and observation. The predictions of Miles' theory are shown in Fig. 10 with the curve designated *M*. This predicted curve is in agreement with none of the data over the frequency range under consideration. A similar conclusion concerning the magnitude of the instability present was reached by Snyder and Cox (1966). The SC curve in Fig. 10 is an empirical relationship for β suggested by Snyder and Cox on the basis of their data; for the case of waves traveling downwind, it is defined by

$$\beta = 2\pi s f(W/c - 1), \tag{13}$$

where s is the ratio of the densities of air and seawater and W is the wind measured at one wavelength above the mean sea surface. Neglecting the upwind run, the agreement between the measurement and the predictions of (13) is quite remarkable.

In Fig. 10 it seems particularly significant that β is positive for waves traveling at phase speeds equal to, or greater than, the wind speed (§ 4.2). Such a result

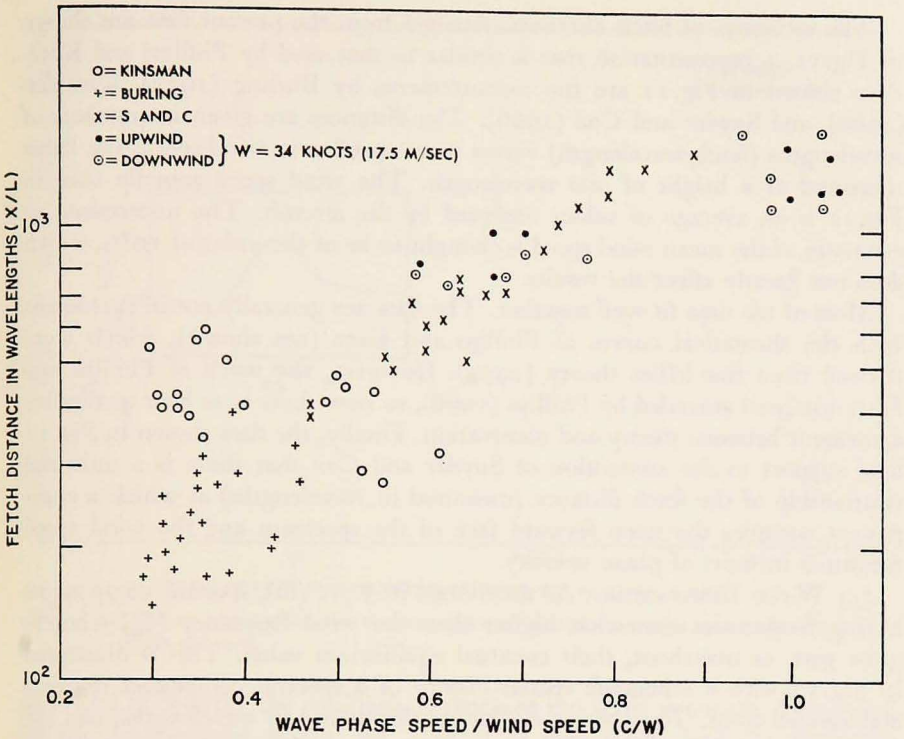

Figure 11. Fetch distances (expressed in wavelengths) at which a component occupies the steep forward face of the spectrum. Also shown are the results of other workers.

is contrary to the predictions of instability theories. One possible explanation for this result has been given by Phillips (1966) and in a more general sense by Hasselmann (in press); the weak coupling of the atmospheric turbulence and the wind-wave fields could produce a positive β for waves moving faster than the wind.

7.2.4 Transition between Linear and Exponential Growth. Of considerable interest is the *transition distance* at which the process of linear growth and exponential growth are equal ($\alpha = \beta F$). As postulated by Phillips and Katz (1961), this is the *fetch distance* required for a particular spectral component to occupy the steep forward face of the energy spectrum. We have used Fig. 10 and the closed-form solution of (4) to arrive at estimates of the transition distance. These were then compared with the fetch distances shown in Fig. 11 (discussed in following paragraph). In 11 out of 13 estimates, the fetch distance was roughly 2 to 4 times greater than the transition distance. The Snyder and Cox data gave a typical factor of 7, but their data were not particularly suitable for the estimate. It appears that the transition distance is not equivalent to the fetch distance.

The estimates of fetch distances obtained from the present data are shown in Fig. 11, a representation that is similar to that used by Phillips and Katz. Also shown in Fig. 11 are the measurements by Burling (1955), Kinsman (1960), and Snyder and Cox (1966). The distances are given in numbers of wavelengths (fetch/wavelength) versus wave speed over wind speed, the latter measured at a height of one wavelength. The wind speed actually used in Fig. 11 is an average of values observed by the aircraft. The uncertainty in estimates of the mean wind speed is thought to be of the order of 10%, which does not greatly affect the results.

Most of the data fit well together. The data are generally not in agreement with the theoretical curves of Phillips and Katz (not shown), which were derived from the Miles theory (1957). However, the work of Phillips and Katz has been amended by Phillips (1966), so now there is at least qualitative agreement between theory and observation. Finally, the data shown in Fig. 11 lend support to the contention of Snyder and Cox that there is a universal relationship of the fetch distance (measured in wavelengths) at which a component occupies the steep forward face of the spectrum and the wind speed measured in units of phase velocity.

7.3 Wave Dissipation. As mentioned in § 7.1 (iii), spectral components having frequencies somewhat higher than the wind frequency (f_w) seem to grow past, or overshoot, their eventual equilibrium value. This is illustrated in Fig. 12 with a schematic spatial history of a spectral component in non-dimensional form. The abscissa is distance downwind in wavelengths, and the ordinate is the value of the component, F, at a given x divided by the maximum value, F_m, achieved by the component throughout its spacial history.

Fig. 12 shows the number of wavelengths (x/L) from the leeward fetch edge at which F_m occurs for the various frequencies. In the data shown for the downwind run, the near-zone peak area previously mentioned has been neglected. Data for only the K_3 directional assumption are presented, but either of the other two spreading factors would have served as well. While there is some scatter in the data, it appears that high-frequency components reach their maximum value in fewer wavelengths than the lower-frequency waves.

It is informative to investigate the correspondence of the observations with proposed frequency power-law formulations in the equilibrium range. Fig. 13 is a log-log plot of wave frequency versus F_m, the maximum spectral value. Only upwind values of F_m have been used. Also included in Fig. 13 are estimates, obtained through averaging, of the eventual equilibrium value, F_e, for both runs.[6] Although neither of the exponents of the estimated best-fit lines can be considered precise, the relative difference between the two lines is significant. A difference in this magnitude occurs for all directional assumptions.

Whatever the ultimate cause of the overshoot effect may be, it does seem to present a partial explanation for the controversy over the form of the representa-

6. F_e/F_m for both runs is between 0.35 to 0.75, with the data badly scattered.

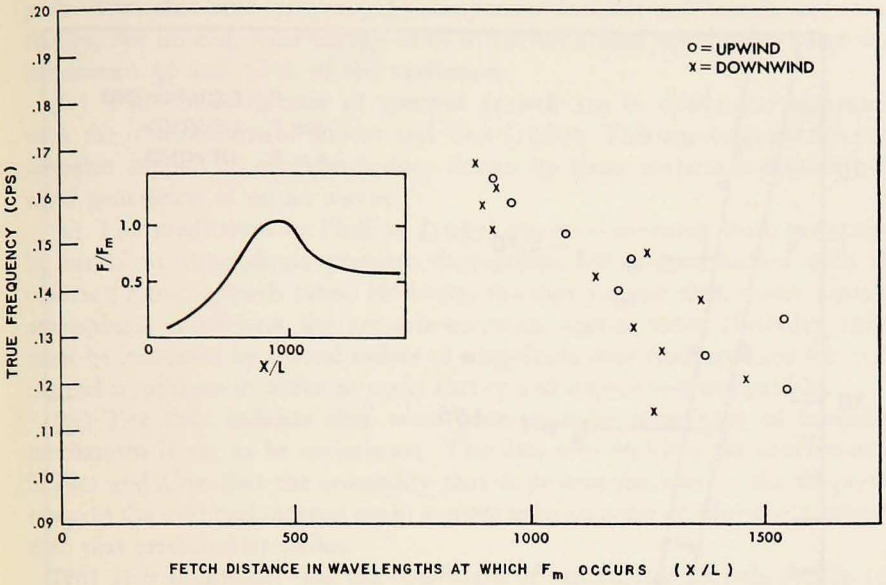

Figure 12. The overshoot effect and the occurrence of spectral component maxima in wavelengths from the coast.

tion used to describe the equilibrium range of the wave spectrum. Depending on the experimental design, the amount of data taken, and the frequency range considered, it would be possible to inadvertently bias the results toward either higher or lower estimates of a pure-power law exponent. It is reasonable to suggest that an explanation such as that given in § 7.1 and a representation of the form (12) will be required in order to describe more fully the establishment and maintenance of spectral equilibrium.

8. *Summary.* By using a modified airborne radar altimeter it has been possible to obtain sequential estimates of fetch-limited wave spectra. Since these spectra are representative of fetch distances from 5 to 350 km, it has been possible to simultaneously follow the development of a *number* of spectral components from their very beginnings to their final equilibrium state. Although these data were taken under only one typical wind condition, they still provide additional insight into the processes of wave generation and dissipation. The more important results of this paper may be summarized as follows:

(i) The peak of the spectrum moves toward lower frequencies with distance from the lee shore.

(ii) Energy is being transmitted simultaneously to the entire frequency range of the spectrum.

(iii) A particular spectral component, of frequency somewhat higher than the wind frequency, grows until it has occupied the position of the spectral

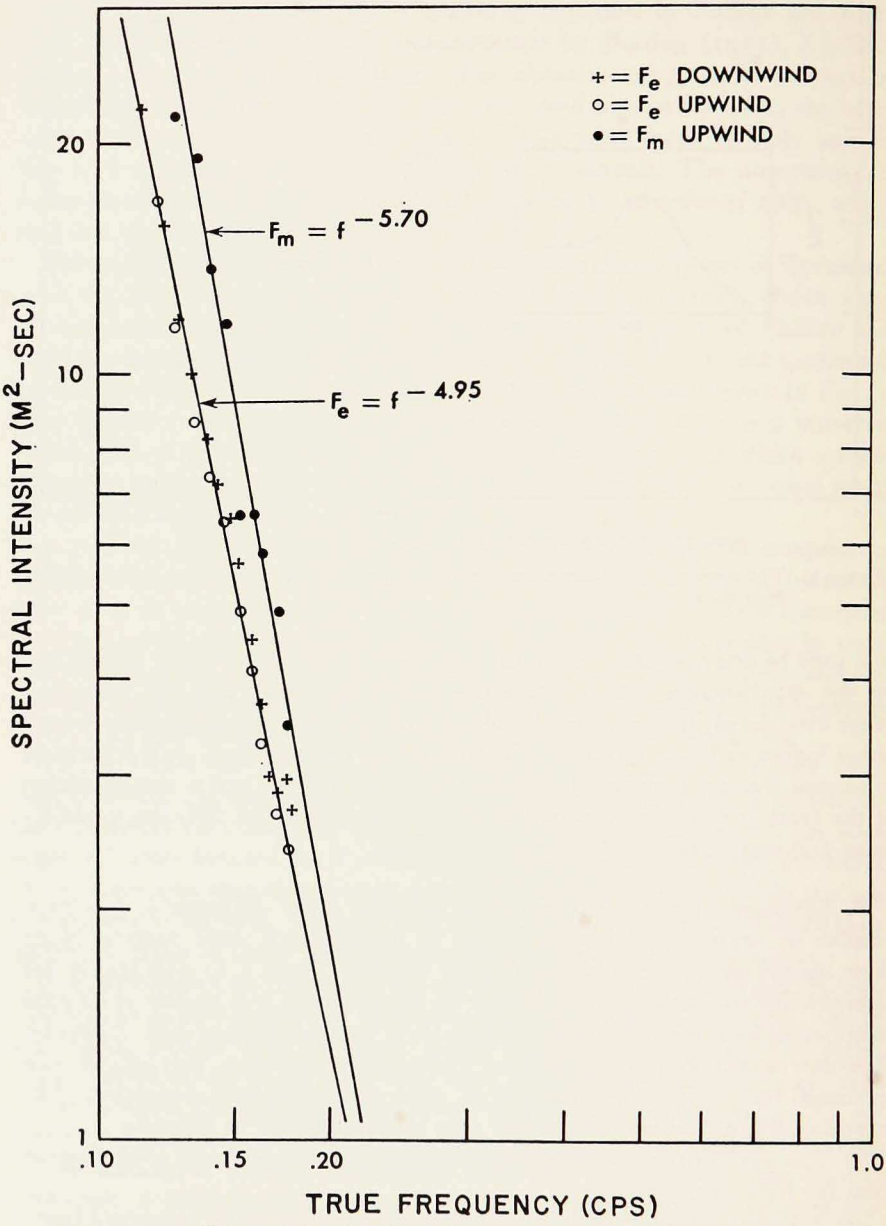

Figure 13. Log-log plot of F_m and F_e vs wave frequency.

peak. After that time (distance) the component does not maintain its maximum energy, but instead, loses energy until it reaches a final equilibrium value that is between 30 and 70% of the maximum.

(iv) The observed rates of spectral growth are in substantial agreement with the observations of Snyder and Cox (1966). This agreement lends considerable support to the conclusions drawn by those authors concerning the wind generation of ocean waves.

(v) The predictions in Phillips' (1957) theory concerning wave generation by turbulent atmospheric pressure fluctuations are in good accord with the observed linear growth rates. However, the data suggest that, under unstable atmospheric conditions, the pressure-spectrum scaling factor (Priestley 1965) must be increased by several orders of magnitude over that expected for near-neutral conditions in order to make theory and experiment compatible.

(vi) The data indicate that wave generation by some type of instability mechanism is yet to be understood. The data also reaffirm the conclusion of Snyder and Cox that the instability that is present (at least in the frequency range of the eventual spectral peak) appears to be an order of magnitude stronger than that predicted by Miles.

(vii) It is significant that the coefficient of exponential growth, β (Fig. 10), is positive for waves having phase speeds equal to, or greater than, the wind speed.

(viii) Estimates of the fetch distance, where a component occupies the steep forward face of the spectrum, are in good agreement with other data. The observations also indicate that these fetch distances are 2 to 4 times greater than the transition distance as defined by Phillips and Katz (1961).

Acknowledgments. Thanks are due Charles Cox, Blair Kinsman, Walter Munk, and Owen Phillips for providing fruitful discussions during the course of this project. Special gratitude is extended to Russ Snyder for his valuable suggestions and the critical reading of this paper. Acknowledgments are also due L. S. Simpson, who was an excellent sounding board and assisted in weather forecasting, and to Gary Athey, who performed tirelessly on our behalf. The work described in this paper would not have been possible without the capable efforts of the crew of the ASWEPS aircraft, El Coyote. A final and heartfelt thanks to J. Barnett for much more assistance than should have been expected.

REFERENCES

Baer, Ledolph

1963. An experiment in numerical forecasting of deep water ocean waves. Lockheed-California Co., 17501. 51 pp.

Barnett, T. P.

1966. On the generation, dissipation and prediction of ocean wind waves. Ph.D. dissertation, Univ. of California, San Diego; 190 pp.

BARNETT, T. P., and J. C. WILKERSON
1967. On the interpretation of fetch-limited wave spectra as measured by an airborne sea-swell recorder. Tech. Rep. U.S. Naval Oceanogr. Office, 191; 54 pp.

BLACKMAN, R. B., and J.W. TUKEY
1958. The measurement of power spectra. Dover Press, New York. 190 pp.

BURLING, R.W.
1955. Wind generation of waves on water. Ph.D. dissertation, Imperial Coll., Univ. of London; 181 pp.

CARTWRIGHT, D. E.
1963. The use of directional spectra in studying the output of a wave recorder on a moving ship, *In* Ocean Wave Spectra, pp. 203–218. Prentice Hall, Inc., New Jersey. 357 pp.

COTE, L. J., J. O. DAVIS, WILBUR MARKS, R. J. MCGOUGH, EMANUEL MEHR, W. J. PIERSON, JR., J. F. ROPEK, GEORGE STEPHENSON, and R. C. VETTER
1960. The directional spectrum of a wind generated sea as determined from data obtained by the stereo wave observation project, Met. Pap. N.Y. Univ., 2 (6); 88 pp.

DE LEONIBUS, P. S.
Measurements of momentum flux at Argus Island tower, Bermuda. In preparation.

HASSELMANN, KLAUS
1960. Grundgleichungen der seegangsvoraussage. Schiffstechnik, *7*: 191–195.
Weak interaction theory of ocean waves. Manuscript.

HIDY, G. M.
1965. The growth of wind waves on water in a channel. NCAR ms., *66*; 18 pp.

KINSMAN, BLAIR
1960. Surface waves at short fetch and low wind speed—a field study. Techn. Rep. Chesapeake Bay Inst., *19*; 169 pp.

LONGUET-HIGGINS, M. S., D. E. CARTWRIGHT, and N. D. SMITH
1963. Observations of the directional spectrum of sea waves using the motions of a floating buoy; *In* Ocean Wave Spectra, pp. 111–132. Prentice Hall, Inc., New Jersey. 357 pp.

MILES, J.W.
1957. On the generation of surface waves by shear flows. Part I. J. fluid Mech., *3*: 185–204.

MUNK, W. H., G. R. MILLER, F. E. SNODGRASS, and H. F. BARBER
1963. Directional recording of swell from distant storms. Philos. Trans. roy. Soc., *255*: 505–584.

NEUMANN, GERHARD, and W. J. PIERSON, JR.
1963. Comments, *In* Ocean Wave Spectra, p. 13. Prentice Hall, Inc., New Jersey. 357 pp.

PHILLIPS, O. M.
1957. On the generation of waves by turbulent wind. J. fluid Mech., *2*: 417–445.
1958a. Wave generation by turbulent wind over a finite fetch. Proc. 3rd U.S. nat. Congr. appl. Mech., Amer. Soc. Mech. Engng.; 785–789.
1958b. The equilibrium range in the spectrum of wind generated waves. J. fluid Mech., *4*: 426–434.
1963. Comments, *In* Ocean Wave Spectra, p. 34. Prentice Hall, Inc., New Jersey. 357 pp.
1966. Dynamics of the upper ocean, pp. 119–122. Camb. Univ. Press; 257 pp.

PHILLIPS, O. M., and E. J. KATZ
1961. Low frequency components of the spectrum of wind generated waves. J. Mar. Res., *19*: 57–69.

PIERSON, W. J., JR., GERHARD NEUMANN, and R.W. JAMES
1955. Observing and forecasting ocean waves. Publ. U.S. Hydrogr. Off., *603*: 284 pp.

PRIESTLEY, J. T.
1965. Correlation studies of pressure fluctuations on the ground beneath a turbulent boundary layer. Rep. nat. Bur. Stand., *8942*; 92 pp.

REDISH, K. A.
1961. An introduction to computational methods. John Wiley and Sons, Inc., New York. 211 pp.

SNYDER, R. L.
1965. The wind generation of ocean waves. Ph.D. dissertation, Univ. of California, San Diego; 393 pp.

SNYDER, R. L., and C. S. COX
1966. A field study of the wind generation of ocean waves. J. Mar. Res., *24*: 141–178.

ST. DENIS, MANELY, and W. J. PIERSON, JR.
1953. On the motions of ships in confused seas. Trans. Soc. nav. Arch. Mar. Engr., *61*: 332–357.

APPENDIX

Growth of the downwind component of the spectrum as a function of true wave frequency (f), directional assumption (K), and distance from the coast. Note, the distance is given in nautical miles (1 n.m. = 1.853 km). The x's and o's are data from the downwind and upwind runs, respectively.

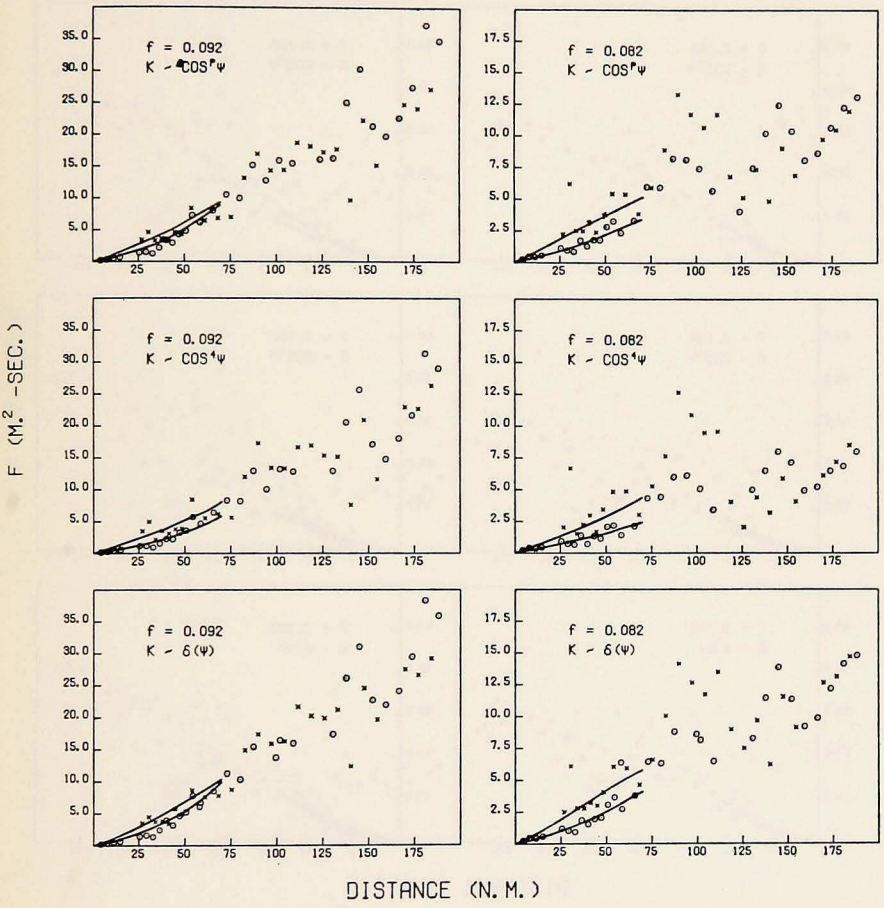
f = 0.092
K ~ COS⁴Ψ
f = 0.082
K ~ COS⁴Ψ
f = 0.092
K ~ COS⁴Ψ
f = 0.082
K ~ COS⁴Ψ
f = 0.092
K ~ δ(Ψ)
f = 0.082
K ~ δ(Ψ)
F (M.² -SEC.)
DISTANCE (N. M.)

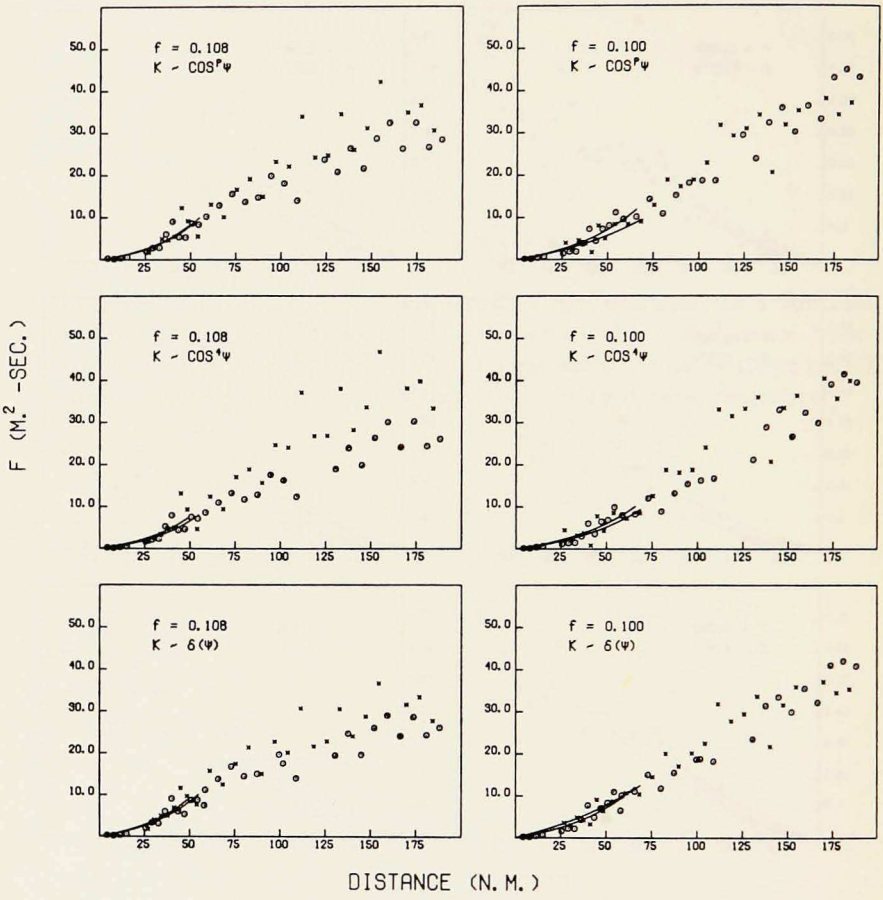
f = 0.108
K ~ COS^P Ψ
f = 0.100
K ~ COS^P Ψ
f = 0.108
K ~ COS^4 Ψ
f = 0.100
K ~ COS^4 Ψ
f = 0.108
K ~ δ(Ψ)
f = 0.100
K ~ δ(Ψ)
50.0
40.0
30.0
20.0
10.0
25
50
75
100
125
150
175
F (M.2 -SEC.)
DISTANCE (N. M.)

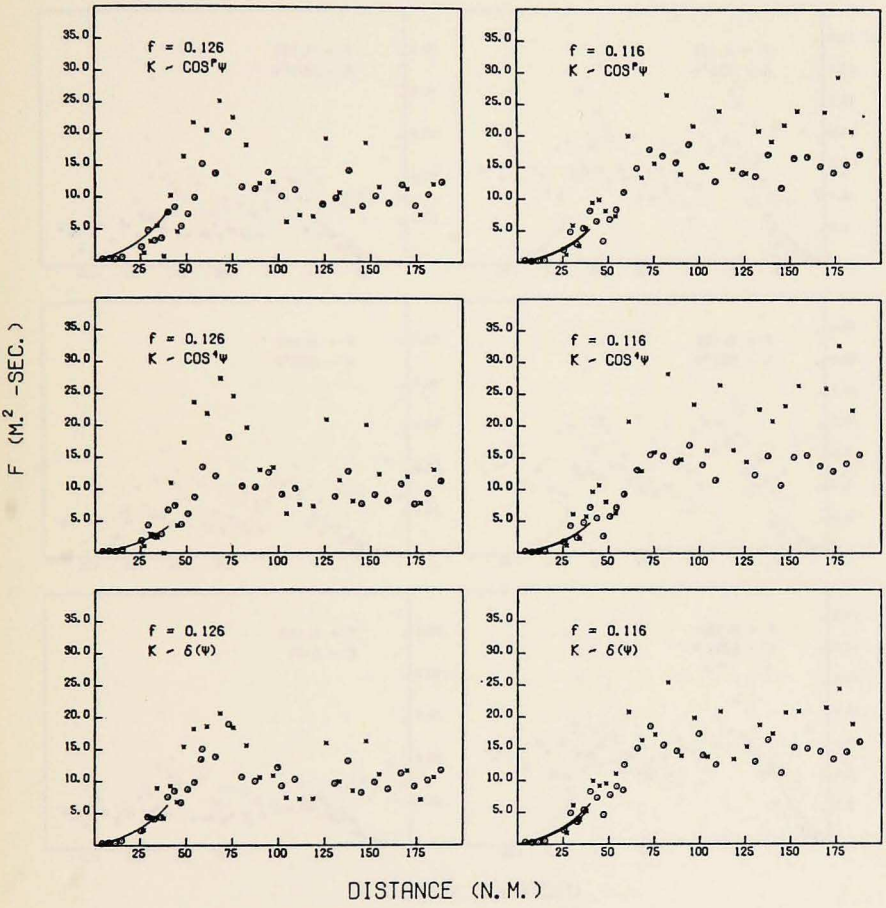
f = 0.126
K ~ COS²ψ
f = 0.116
K ~ COS²ψ
f = 0.126
K ~ COS⁴ψ
f = 0.116
K ~ COS⁴ψ
f = 0.126
K ~ δ(ψ)
f = 0.116
K ~ δ(ψ)
35.0
30.0
25.0
20.0
15.0
10.0
5.0
25
50
75
100
125
150
175
F (M.² -SEC.)
DISTANCE (N. M.)

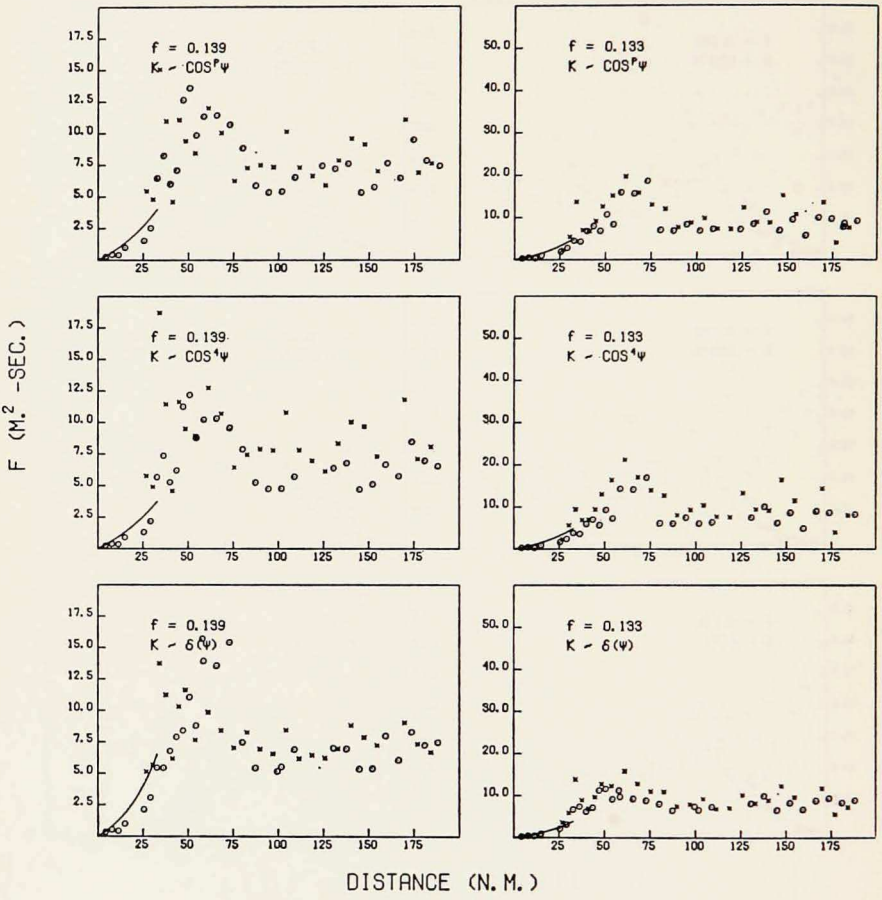
f = 0.139
K ~ COS²Ψ
f = 0.133
K ~ COS²Ψ
f = 0.139
K ~ COS⁴Ψ
f = 0.133
K ~ COS⁴Ψ
f = 0.139
K ~ δ(Ψ)
f = 0.133
K ~ δ(Ψ)
F (M.² -SEC.)
DISTANCE (N. M.)

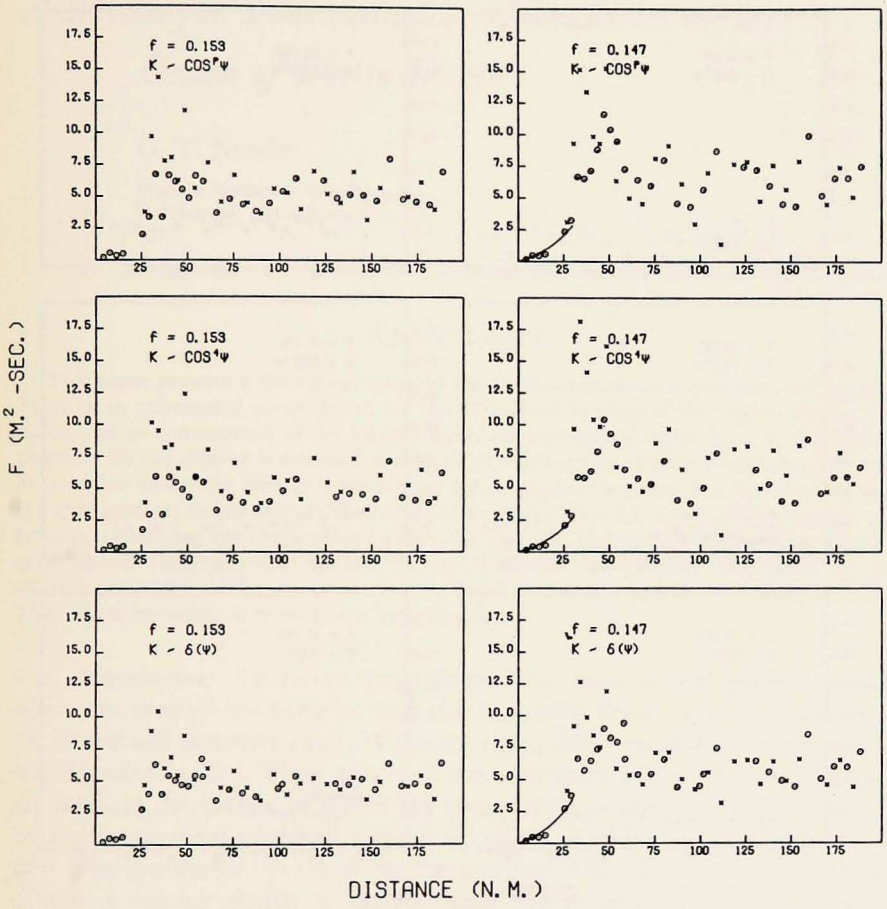
f = 0.153
K ~ COS²Ψ
f = 0.147
K ~ COS²Ψ
f = 0.153
K ~ COS⁴Ψ
f = 0.147
K ~ COS⁴Ψ
f = 0.153
K ~ δ(Ψ)
f = 0.147
K ~ δ(Ψ)
17.5
15.0
12.5
10.0
7.5
5.0
2.5
25
50
75
100
125
150
175
F (M.² -SEC.)
DISTANCE (N. M.)

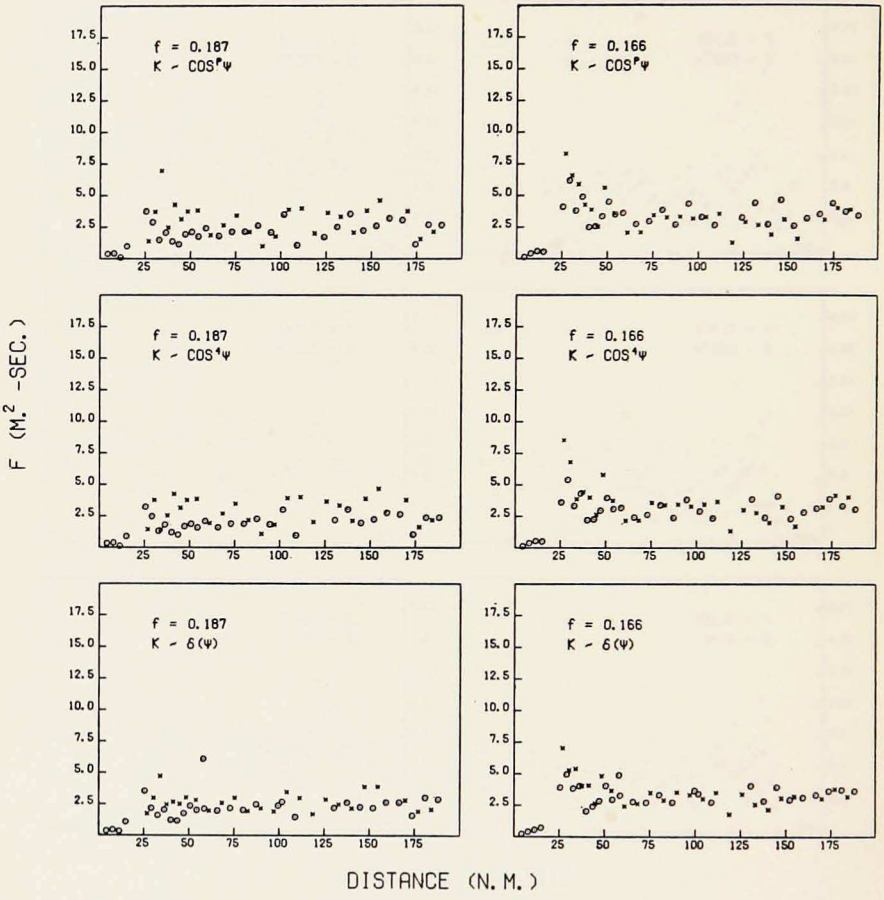
f = 0.187
K ~ COS²Ψ
f = 0.166
K ~ COS²Ψ
f = 0.187
K ~ COS⁴Ψ
f = 0.166
K ~ COS⁴Ψ
f = 0.187
K ~ δ(Ψ)
f = 0.166
K ~ δ(Ψ)
F (M.² -SEC.)
DISTANCE (N. M.)